Effect of lanthanum on the catalytic properties of PtSn/γ-Al$_2$O$_3$ bimetallic catalysts prepared by successive impregnation and controlled surface reaction

G. Del Angel,[a,*] A. Bonilla,[a] Y. Peña,[a] J. Navarrete,[b] J.L.G. Fierro,[c] and D.R. Acosta [b,1]

[a] *Universidad Autónoma Metropolitana-Iztapalapa, Departamento de Química, PO Box 55-534, CP 09340 México, DF, Mexico*
[b] *Instituto Mexicano del Petróleo, Eje Central Lázaro Cárdenas 152, AP 14-805, CP 07730 México, DF, Mexico*
[c] *Instituto de Catálisis y Petroquímica, CSIC, Cantoblanco, 28049 Madrid, Spain*

Abstract

Bimetallic PtSn/γ-Al$_2$O$_3$–La$_2$O$_3$ catalysts were prepared by two comparative methods, successive impregnation (SI) and controlled surface reaction (CSR). FTIR-pyridine adsorption revealed a decrease in support acidity as a function of lanthanum content. Oxidized Pt^{2+} was identified by CO-FTIR chemisorption and by XPS spectra on catalysts prepared by SI. When the CSR preparation method was used, reduced Pt^0 was observed and oxidized Pt^{2+} was not detected. As the lanthanum content increased a diminution in cyclohexane dehydrogenation and *n*-heptane conversion was observed. Low hydrogenolysis and high selectivity to C$_7$-olefins were obtained in both preparations. It is proposed that lanthanum in SI catalysts stabilizes the platinum in an oxidation state, Pt^{2+}, and diminishes the support acidity. In CSR preparations the lanthanum effect is limited to inhibit the support acidity and hence to the bifunctional reactions occurring during the *n*-heptane conversion.

1. Introduction

Bimetallic catalysts are widely used in industrial processing. It has been largely reported that when Sn is added to Pt/γ-Al$_2$O$_3$ catalysts, despite a loss in activity, a large stability is obtained in reforming of naphtha [1,2]. Moreover, bimetallic platinum–tin catalysts have been also widely reported as active in paraffin dehydrogenation reactions [3–7]. The catalytic dehydrogenation of alkanes is of great industrial importance for their applications in processes such as polymerization and alkylation and in petrochemical products. It is then interesting to make use of previous knowledge to prepare or modify PtSn reforming catalysts to obtain new and promising catalysts with high olefin yields during *n*-heptane conversion. Previous studies have investigated the

support effect on the reduction behavior of bimetallic PtSn catalysts useful for alkane dehydrogenation; supports such as Al$_2$O$_3$, SiO$_2$, and ZrO$_2$ have been studied [8–11]. However, with regard to alkane dehydrogenation reactions, few studies have concerned the support effect when the support contains lanthanides. It has been reported that the main role of La$_2$O$_3$ on γ-Al$_2$O$_3$ is to improve the thermal stability of the support. The support stabilization is attributed to the LaAlO$_3$ formation [12]. However, a modification of the Al$_2$O$_3$ properties with lanthanides leads to a modification in their acidic/basic properties [13,14], and hence the activity of supported metal catalysts can be modified by metal–support interaction effects.

The catalytic properties of the PtSn bimetallic catalysts strongly depend on the preparation method used. In previous work [15], we observed that when Boehmite was first impregnated with La(NO$_3$)$_3$ · 6H$_2$O and then impregnated with platinum and tin, a strong interaction between metals and support occurred. Characterization by various techniques showed the formation of Pt–SnO–La$_2$O$_3$ multiple

* Corresponding author. San Rafael Atlizco 186, CP 09340, Col Vicentina, AP 55-534 México, DF, Mexico
E-mail address: gdam@xanum.uam.mx (G. Del Angel).
[1] On sabbatical leave from IFUNAM.

phases where platinum Pt^{2+} was observed. In the present work we report the results obtained by comparing Pt–Sn–La_2O_3–Al_2O_3 bimetallic catalysts prepared by successive impregnation (SI) with those prepared by controlled surface reaction (CSR), with the aim of understanding the role of lanthanum in n-heptane dehydrogenation.

2. Experimental

2.1. Chemicals

$La(NO_3)_3 \cdot 6H_2O$ (Stream, 99.999%), $H_2PtCl_6 \cdot 6H_2O$ (Stream, 99.9%), $SnCl_4 \cdot 5H_2O$ (Baker, 99.9%), $Sn(C_4H_9)_4$ (Stream 94%), n-heptane (Aldrich, 99%), and cyclohexane (Aldrich, 99%), were used. UHP hydrogen from AGA was also used for all catalytic experiments.

2.2. Supports

The γ-Al_2O_3 reference support was prepared by calcination of Boehmite Catapal B under air flow at 500 °C; the surface area was 221 m^2/g. The γ-Al_2O_3 lanthanum-doped supports were prepared by impregnation of Boehmite with the appropriate amount of a $La(NO_3)_3 \cdot 6H_2O$ solution to obtain 1, 10, and 20 wt% La. The solids were then calcined under air flow at 650 °C. The surface areas of these solids were 171, 170, and 112 m^2/g, respectively.

2.3. X-ray diffraction spectra

X-ray diffraction patterns of supports γ-Al_2O_3, γ-Al_2O_3–1La, γ-Al_2O_3–10La, and γ-Al_2O_3–20La were obtained at room temperature using a Siemens D-500 X-ray powder diffractometer coupled to a copper anode tube. The K_α radiation was selected with a diffracted beam monochromator. An angular range 2θ from 2 to 70° was recorded using step scanning and long counting times to determine the positions of the γ-Al_2O_3 peaks.

2.4. Catalyst preparation

A reference Pt catalyst (P/A) was prepared by wet impregnation of the γ-alumina support with a $H_2PtCl_6 \cdot 6H_2O$ chloride solution (HCl pH 2). The catalyst was then dried and calcined at 500 °C under air flow; the catalyst was reduced under H_2 flow at 500 °C for 5 h.

Bimetallic PtSn reference catalyst was prepared by successive impregnation as follows: The calcined monometallic Pt catalyst was impregnated with $SnCl_4 \cdot 5H_2O$ in an acidic HCl solution (pH 2), after the catalyst was dried, calcined, and then reduced under H_2 flow for 5 h at 500 °C. For PtSn catalysts prepared by CSR [16–18], $Sn(n$-$C_4H_9)_4$ was dissolved in n-heptane and purged with N_2. This solution was put in contact with the reduced monometallic P/A catalyst

at 70 °C and maintained for 8 h under constant stirring. Afterward, the solid was filtered and washed with n-heptane to eliminate the weakly adsorbed tin. Finally, the catalyst was dried and reduced with H_2 at 500 °C for 5 h. For PtSn alumina-doped catalysts we followed the same protocol as that used for the reference catalysts but used γ-Al_2O_3–La_2O_3 instead of γ-Al_2O_3.

The nominal contents of Pt and Sn were 0.5 and 0.3 wt%, respectively (corresponding to a Sn/Pt molar ratio of 1). The Pt and Sn contents were determined by plasma spectroscopy, and the chloride content was determined by a volumetric technique. Results are reported in Table 1.

The catalysts were labeled as follows: P/A for platinum supported on alumina, and PS/A for platinum–tin supported on alumina. Catalysts are marked as 1La, 10La, and 20La, indicating the amount of wt% La contained in the support; SI and CSR labels refer to the preparation method. For instance, PS/A–1La–SI corresponds to PtSn prepared by successive impregnation on γ-Al_2O_3 doped with 1 wt% La.

2.5. Electron microscopy

The powder samples were ground softly in an agate mortar, dispersed in isopropylic alcohol, and deposited on 200-mesh copper grids covered with a holey carbon film. High-resolution and conventional electron microscope observations were carried out in a JEOL 4000 EX electron microscope equipped with a pole piece with spherical aberration coefficient of CS = 1.00 mm. Electron micrographs were recorded with a TV-like system and on conventional electron microscopy negative film.

2.6. FTIR measurements

The FTIR spectra of adsorbed CO were recorded using a Nicolet-FX710 apparatus at room temperature. The samples were pressed into thin wafers and placed in a Pyrex glass cell equipped with CaF_2 windows. The samples were reactivated in situ at 400 °C for 30 min under vacuum (10^{-6} Torr). CO admission was carried out at 200 °C and 20 Torr; afterward the cell was cooled to room temperature, the excess CO was evacuated over 30 min, and the CO absorption spectra were recorded.

The FTIR-pyridine adsorption technique was used to determine the acidity of the γ-Al_2O_3 and γ-Al_2O_3–La supports with the same apparatus mentioned above. The samples were pretreated in situ at 400 °C for 30 min under vacuum and then cooled to room temperature. Nitrogen saturated with pyridine was passed over the sample for 30 min. Afterward, the excess of pyridine was pumped out for 30 min, and the pyridine absorption spectra were recorded at room temperature and desorbed at different temperatures.

2.7. XPS analysis

A VR Escalab 200R electron spectrometer equipped with hemispherical analyzer equipment was used for the XPS studies. The spectrometer was operated in a constant pass energy mode, and a nonmonochromatized Mg-K$_\alpha$ ($h\nu = 1253.6$ eV, 1 eV $= 1.603 \times 10^{-9}$ J) X-ray source operated at 10 mA and 12 kV. All samples were reduced in situ under hydrogen at 300 °C for 1 h. A PDP 11/04 computer (Digital Co.) was used to record and analyze the spectra. The intensities of the peaks were estimated by calculating the integral of each peak after subtracting an S-shaped background and fitting the experimental peak to a combination of Lorentzian/Gaussian lines of variable proportions. The binding energies (BE) were referenced to the Al 2p peak, the BE of which was fixed at 74.5 eV.

2.8. Catalytic activity

The catalytic activity of the cyclohexane dehydrogenation was determined at 300 °C and that of the *n*-heptane conversion at 490 °C, using a conventional flow reactor under differential mode (low conversions < 15%). Reaction conditions for cyclohexane dehydrogenation were partial pressures of cyclohexane and hydrogen, 48.2 and 711.8 Torr, respectively. For *n*-heptane conversion the partial pressures were 11 Torr for *n*-heptane and 749 Torr for hydrogen. The hydrogen saturated with the reactants was passed through the reactor; the products were analyzed with an online gas chromatograph, equipped with crosslinked methylsiloxane column of 50 m × 0.2 mm × 0.5 μm. The products were identified with a HP-GC-MS 5973 gas chromatograph mass spectrometer.

3. Results

3.1. X-ray diffraction analysis

The X-ray diffraction patterns of calcined Boehmite and calcined Boehmite impregnated with La(NO$_3$)$_3 \cdot$ 6H$_2$O are shown in Fig. 1. The characteristic peaks of γ-Al$_2$O$_3$ can
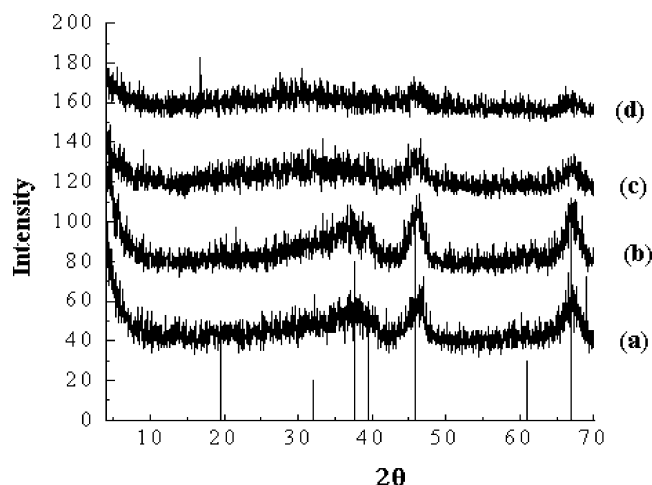
Fig. 1. XRD patterns of the supports: (a) γ-Al$_2$O$_3$, (b) γ-Al$_2$O$_3$–1La, (c) γ-Al$_2$O$_3$–10La, (d) γ-Al$_2$O$_3$–20La.

be seen in Fig. 1a. In the support containing La$_2$O$_3$ (1% La) we do not observe any modification of the diffraction pattern of γ-Al$_2$O$_3$ (Fig. 1b). However, at 10La content, the X-ray diffraction pattern (Fig. 1c) showed a decrease in typical alumina peaks until they began very small in 20% La content (Fig. 1d). The absence of La$_2$O$_3$ characteristic peaks in the spectra suggested that the La$_2$O$_3$ was incorporate in the network of the Al$_2$O$_3$, or that La$_2$O$_3$ is highly dispersed on the alumina surface; therefore it could not be observed by XRD.

3.2. Catalysts characterization

As mentioned before, the PtSn catalysts were prepared by successive impregnation and controlled surface reaction. In both preparations tin was added to a Pt base catalyst supported on γ-Al$_2$O$_3$ and γ-Al$_2$O$_3$–La with different lanthanum loads.

Table 1 gives the Pt, Sn, and Cl weight concentrations. The platinum content for all catalysts varies between 0.37 and 0.5 wt%. For SI catalysts, tin load was between 0.27 and 0.51 wt% and for CSR preparation the tin load was maintained between 0.08 and 0.13 wt%.

Table 1

Characterization and catalytic activity at 300 °C for cyclohexane dehydrogenation over Pt and PtSn supported on Al$_2$O$_3$ and Al$_2$O$_3$–La catalysts

Catalyst	wt%			Rate	Particle size TEM
	Pt	Sn	Cl	($\times 10^6$ mol/(s g))	(nm)
P/A [a]	0.49	–	0.39	117	2.3
PS/A–SI	0.37	0.51	0.33	114	–
PS/A–1La–SI	0.45	0.27	0.41	52.3	–
PS/A–10La–SI	0.38	0.43	0.6	39.4	2.5
PS/A–20La–SI	0.44	0.38	4.0	2.4	–
PS/A–CSR	0.46	0.11	0.35	4.6	–
PS/A–1La–CSR	0.5	0.08	0.6	4.2	–
PS/A–10La–CSR	0.38	0.10	0.47	4.9	2.3
PS/A–20La–CSR	0.46	0.13	0.73	4.3	–

[a] Dispersion determined by CO chemisorption (stoichiometry: CO/Pt = 1): 52%D [15].

The chlorine content was estimated between 0.33 and 0.7 wt% for all samples except for the 20 wt% La sample that was prepared by SI, where the content of Cl was 4.0 wt%. A similar result was observed with PtSn/γ-Al$_2$O$_3$–La catalysts prepared by coimpregnation [15]. It has been reported that lanthanides have the ability to retain chlorine on the surface [19,20].

3.3. Electron microscopy

The mean particle size was calculated from conventional electron micrographs using the expression $d_s = \sum n_i d_i^3 / \sum n_i d_i^2$, where d_i is the diameter measured directly from the electron micrographs and n_i is the number of particles having the diameter d_i. Mean particle size determination and high-resolution electron microscopy analysis were carried out for three selected catalysts. The monometallic P/A, the bimetallic PS/A–10La–SI, and PS/A–10La–CSR catalysts showed mean particle sizes of 2.3, 2.5, and 2.3 nm, respectively (Table 1). Micrographs of conventional transmission electron microscopy (CTEM) are shown in Figs. 2 and 3 for PS/A–10La–SI and PS/A–10La–CSR catalysts. In Figs. 4, 5, and 6, HREM (high-resolution electron microscopy) images are shown for P/A and the bimetallic PS/A–10La–SI and PS/A–10La–CSR catalysts.

3.4. Cyclohexane dehydrogenation activity

The activity of cyclohexane aromatization was reported as an indirect way of determining the metallic active surface area. Insensitive structure reactions such as cyclohexane aromatization and benzene hydrogenation are good alternatives to determining the active metallic surface area in catalysts when lanthanides are present [21,22].

For the current catalysts, the indirect accessible metallic areas of PtSn catalysts were obtained by measuring the activity of cyclohexane dehydrogenation at 300 °C. The results
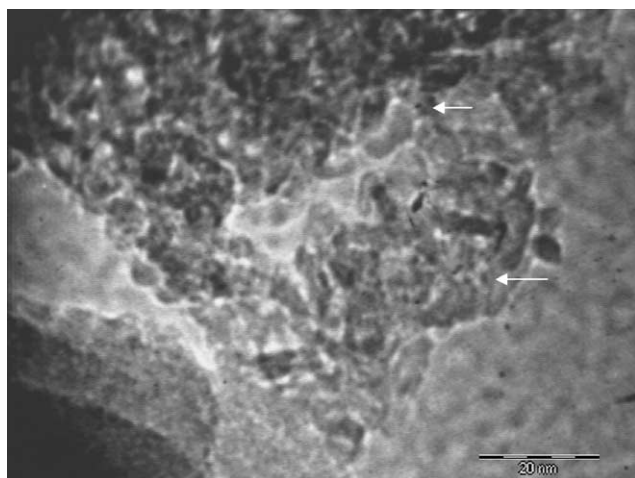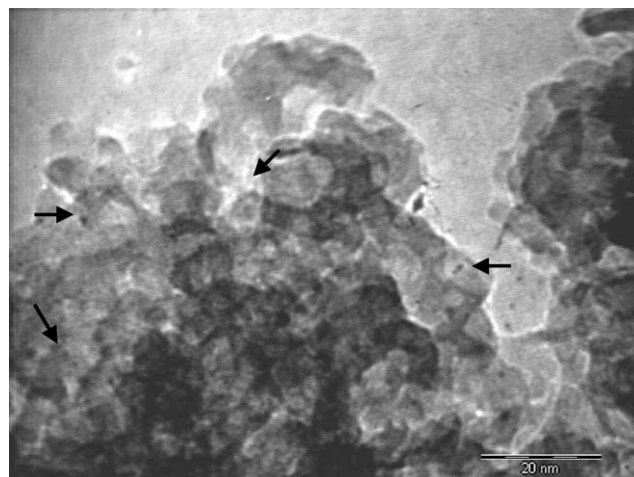

Fig. 3. CTEM micrograph where the metallic phase, marked with black arrow, can be observed in several zones for PS/A–10La–CSR catalyst.
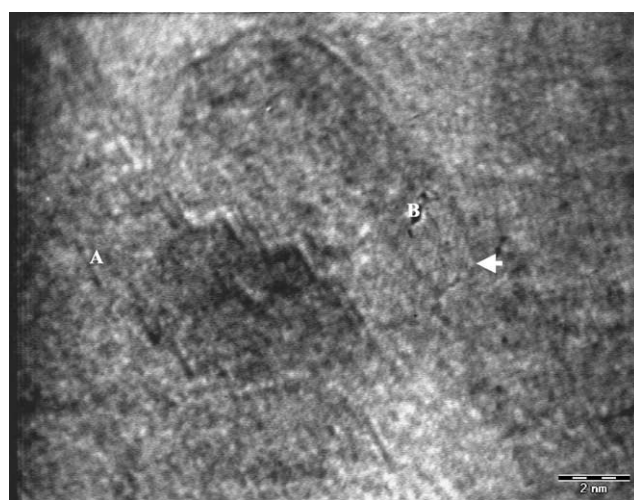

Fig. 4. Electron micrograph showing a set of small crystallites in the zone marked A and showing the profile of a small metallic particle with lattice resolution in the zone marked B for P/A catalyst.
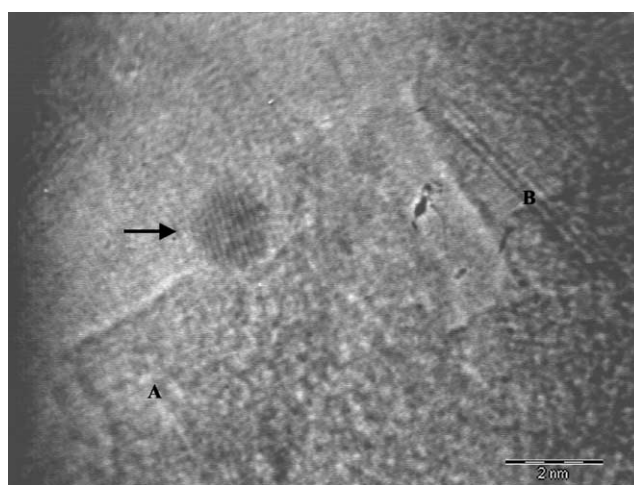

Fig. 2. A conventional transmission electron microscopy (CTEM) micrograph from a PS/A–10La–SI sample where the metallic supported phase can be identified as small darker spots indicated with white arrows.

Fig. 5. HREM micrograph from sample PS/A–10La–SI. A faceted platinum particle together with laminate configurations marked with A and B can be observed.
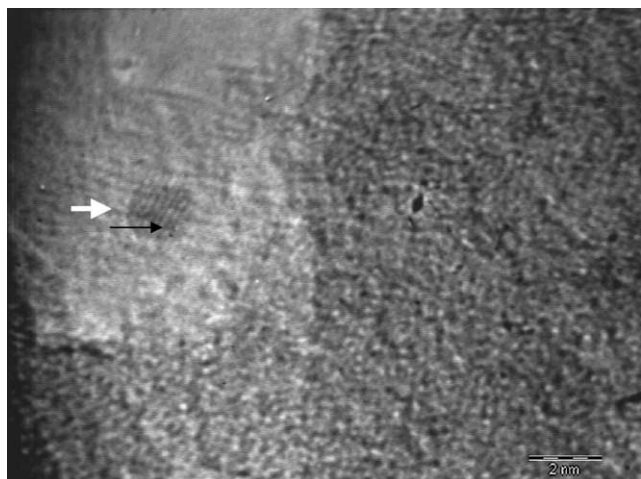
Fig. 6. HREM micrograph from sample PS/A–10La–CSR. A faceted white arrowed platinum particle can be observed in the image.

are reported in Table 1. The rate is reported in mol/(s g). Monometallic catalyst P/A shows the highest activity with a value of 117×10^{-6} mol/(s g).

In SI preparations the addition of Sn to Pt catalyst does not modify the activity, 114×10^{-6} mol/(s g) (PS/A–SI). However, the presence of La on these catalysts produces a decrease in the activity in terms of the La contents in the support, i.e., 52.3×10^{-6}, 39.4×10^{-6}, and 2.4×10^{-6} mol/(s g) for 1, 10, and 20 wt% La, respectively. The rate for cyclohexane dehydrogenation is strongly inhibited by the La content.

On the other hand, in CSR catalysts when Sn was added to platinum catalyst (P/A) a notable decrease in activity of ∼20 times is observed in the bimetallic catalysts. An activity decay from 117×10^{-6} mol/(s g) for P/A catalyst to 4.6×10^{-6} mol/(s g) for PS/A–CSR catalyst was observed. The amount of La in these catalysts series does not modify the activity, since values of 4.2×10^{-6}, 4.9×10^{-6}, and 4.3×10^{-6} mol/(s g) for 1, 10, and 20 wt% La contents, respectively, were found.

3.5. FTIR-pyridine chemisorption

The infrared spectra of adsorbed pyridine are shown in Fig. 7a for γ-Al$_2$O$_3$, Fig. 7b for γ-Al$_2$O$_3$–1La, and Fig. 7c for γ-Al$_2$O$_3$–20La. FTIR-pyridine adsorption is used to determine the type of acid sites. Generally, in the IR spectrum of pyridine adsorption on solids, absorption bands around 1590, 1490, and 1450 cm^{-1} are assigned to the different vibration modes of pyridine adsorbed on Lewis acid sites [23]. The characterization of pyridine adsorbed on Brønsted acid sites is assigned to the absorption band at 1540 cm^{-1} [23].

The spectra corresponding to alumina without lanthanum present three pyridine absorption bands at 1445, 1490, and 1590 cm^{-1} (Fig. 7a): this result shows that only Lewis acidic sites are present. The intensities of the bands gradually decrease as the desorption temperature is increased; at 500 °C, the three bands corresponding to Lewis sites nearly vanish.
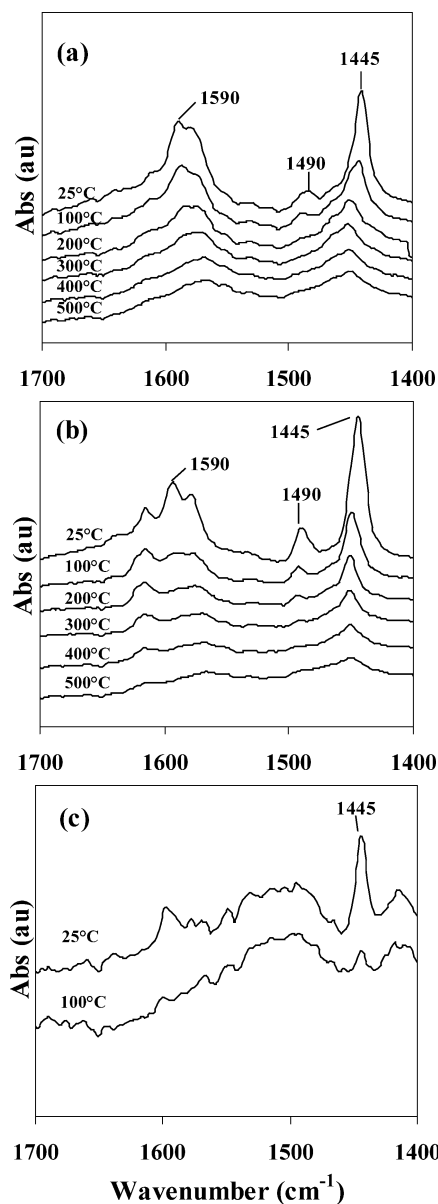

Fig. 7. FTIR spectra of pyridine adsorbed on the samples: (a) γ-Al$_2$O$_3$, (b) γ-Al$_2$O$_3$–1La, (c) γ-Al$_2$O$_3$–20La.

The 1 wt% lanthanum alumina catalyst does not show significant modification of the alumina IR spectra at the different desorption temperatures (Fig. 7b). However, the IR spectra for the 20 wt% La alumina support shows a diminution of the relative intensity of the absorption band at 1445 cm^{-1}, whereas the bands at 1490 and 1590 cm^{-1} are not observed even at room temperature desorption. When the temperature increases above 100 °C, the absorption bands disappeared entirely (Fig. 7c). The absorption band corresponding to the Brønsted acid sites cannot be observed in any support.

3.6. FTIR-CO chemisorption

For catalysts prepared by SI, the IR spectra of adsorbed CO are shown in Fig. 8. The IR spectra of CO adsorbed on
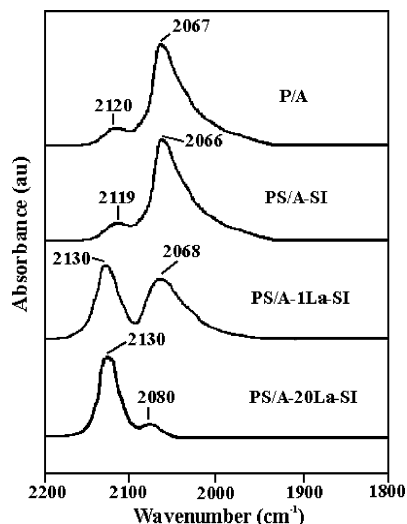
Fig. 8. FTIR spectra of CO adsorbed on different catalysts: P/A, PS/A–SI, PS/A–1La–SI, PS/A–20La–SI.

Fig. 9. FTIR spectra of CO adsorbed on different catalysts: P/A, PS/A–CSR, PS/A–1La–CSR, and PS/A–20La–CSR.

the monometallic P/A and on the bimetallic PS/A–SI catalysts show similar CO-IR position absorption bands at 2067–2066 and 2120–2119 cm^{-1}, assigned to carbon monoxide bonded to platinum atoms in a linear form [24] and to linear CO chemisorbed on Pt atoms on oxidized state, respectively [25–27]. Chlorine effects are not discarded as being responsible for the 2119–2120 cm^{-1} absorption band. Particle size effects in the CO band shift are not considered because, as is shown by electron microscopy, the platinum particle size is of the same order regardless of the preparation method used.

On La-doped bimetallic SI catalysts a shift of the 2066 cm^{-1} band as function of lanthanum content was observed. This peak almost disappeared (2080 cm^{-1}) at the highest La load (20 wt%), while the band at 2119–2130 cm^{-1} assigned to Pt^{+2} progressively increased. The shift of the CO absorption band to higher frequencies (2066 to 2130 cm^{-1}) in the SI preparations can be interpreted as the result of decreasing back donation d$\pi \rightarrow 2\pi^*$ from the metal to the antibonding CO orbitals, due to an interaction of Pt atoms with SnO$_x$ and La$_2$O$_3$, where the Pt is stabilized in an oxidized state (Pt^{2+}). This causes the stretching frequency of the carbonyl group to rise to higher values closer to the gaseous CO frequency [27].

On bimetallic catalysts prepared by CSR (PS/A–CSR) we can also observe a shift of the 2059–2085 cm^{-1} band as a function of lanthanum content. However, compared to SI catalysts the 2119 and 2130 cm^{-1} absorption bands are practically absent (Fig. 9). When the catalysts were prepared by CSR, the platinum was maintained as Pt^0 in the bimetallic catalysts with lanthanum. As mentioned above, in this preparation technique, tin is selectively deposited on the platinum particles and the close contact of Pt and Sn with La$_2$O$_3$ makes it seem that is not occurring. Therefore, the CO-FTIR shift observed as an effect of the lanthanum in SI preparations is not observed here.
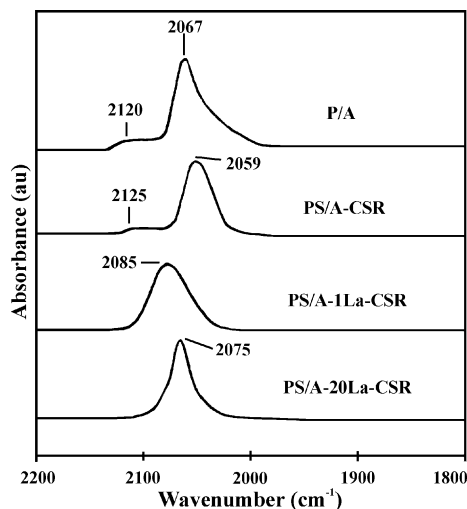
Table 2
Binding energies (eV) of core electrons of Pt and Pt–Sn catalysts supported on γ-Al$_2$O$_3$ and γ-Al$_2$O$_3$–La catalysts prepared by successive impregnation

Catalyst	Al 2p	Pt 4d$_{5/2}$	Sn 3d$_{5/2}$	La 3d$_{5/2}$
P/A	74.5	315.7	–	–
PS/A–1La–SI	74.5	315.6	486.0 (32)	–
			487.6 (68)	
PS/A–10La–SI	74.5	315.2	485.9 (32)	836.3
			487.5 (68)	
PS/A–20La–SI	74.5	314.7 (50)	485.8 (38)	836.5
		317.3 (50)	487.9 (62)	

Table 3
Binding energies (eV) of core electrons of Pt–Sn catalysts supported on γ-Al$_2$O$_3$ and γ-Al$_2$O$_3$–La catalysts prepared by controlled surface reaction

Catalyst	Al 2p	Pt 4d$_{5/2}$	Sn 3d$_{5/2}$	La 3d$_{5/2}$
PS/A–1La–CSR	74.5	314.7	485.4 (55)	836.6
			488.3 (45)	
PS/A–10La–CSR	74.5	314.8	485.5 (46)	836.2
			488.0 (54)	
PS/A–20La–CSR	74.5	314.6	485.2 (35)	836.4
			487.2 (65)	

3.7. X-ray photoelectron spectroscopy (XPS)

The chemical state of catalyst constituents and their proportions at the catalyst surface were evaluated by photoelectron spectroscopy. The binding energies of Al 2p, Pt 4d$_{5/2}$, Sn 3d$_{5/2}$, and La 3d$_{5/2}$ core levels of SI and CSR series are compiled in Tables 2 and 3, respectively. It is emphasized that the most intense Pt 4f of platinum could not be recorded because it overlaps with the strong Al 2p emission coming from aluminum atoms of the support. For the sake of clarity and to compare line profiles, the Pt 4d$_{5/2}$ levels of series SI and CSR are displayed in Figs. 10 and 12, respectively. Similarly, the Sn 3d core level spectra of SI
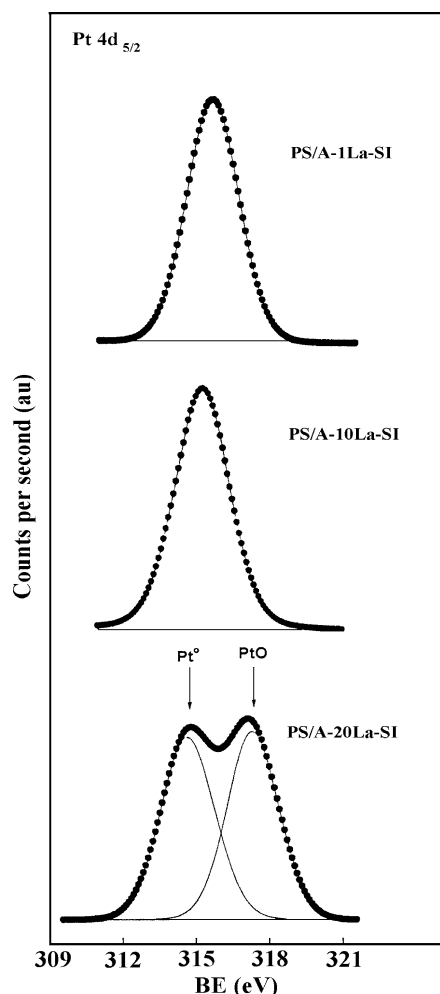
Fig. 10. Pt $4d_{5/2}$ Core level spectra of PS/A–1La–SI, PS/A–10La–SI, and PS/A–20La–SI.

Fig. 11. Sn 3d Core level spectra of PS/A–1La–SI, PS/A–10La–SI, and PS/A–20La–SI.

and CSR series are shown in Figs. 11 and 13, respectively. For all the samples, a small signal at 198.8–199.0 eV, due to chloride ions [28], was detected. In addition, all the La-containing samples exhibited the La $3d_{5/2}$ peak at a binding energy close to 836.2 eV, which is typical of La_2O_3 (Tables 2 and 3) [28].

The binding energy of the Pt $4d_{5/2}$ of the tin-free (Pt/A) sample appeared at 315.7 eV. Binding energies for Pt $4d_{5/2}$ level in alumina-supported catalysts at 315.1 and 316.8 eV for hydrogen-reduced and calcined samples have been assigned to Pt^0 and PtO species, respectively [29,30]. As a matter of fact, the binding energies of core electrons in metallic particles deposited on a high-specific-area carrier show a positive shift, usually 0.3–0.7 eV, with respect the bulk metal. Since the binding energy of Pt $4d_{5/2}$ level in a Pt film (bulk metal) is around 314.4 eV [30], the value of 315.7 eV, which in turn is intermediate between platinum metal and metal oxide, should be ascribed to platinum interacting presumably with some chloride ions retained at the alumina surface. For PtSn bimetallics deposited on alumina modified by 1 and 10% lanthanum and prepared by
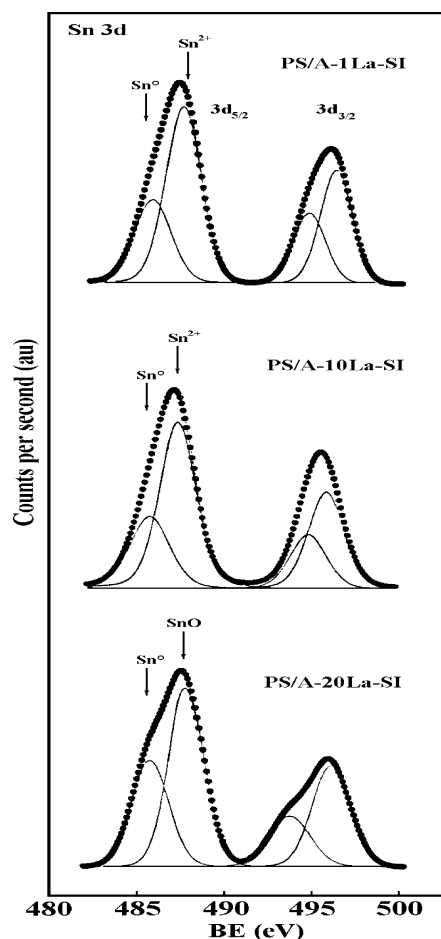
successive impregnation, no change in the binding energy of Pt $4d_{5/2}$ core level was observed. However, for the catalyst containing 20% lanthanum, two components at 314.7 and 317.3 eV appeared. The proportion of these components is the same; their percentages are given in parentheses in Table 2. According to the above, the component at 314.7 eV could be assigned to Pt^0 particles. The other component at 317.3 eV may arise from Pt^{2+} species.

The most intense Sn $3d_{5/2}$ emission from tin showed two components, whose percentages are summarized in Table 2 (see also deconvoluted peaks in Fig. 11). The component at binding energies of 486.0, 485.9, and 485.8 eV for the catalysts modified with 1, 10, and 20% lanthanum, respectively, is associated with a reduced tin phase [31], such as Sn^0 or an alloyed $SnPt_x$ phase with percentages on the order of 32–38%. Another major tin component that exists in the oxidized state (62–68%) at binding energies of 487.6, 487.5, and 487.9 eV is found for PtSn catalysts modified with 1, 10, and 20% lanthanum, respectively.

Binding energies of core electrons of PtSn catalysts prepared by CSR are compiled in Table 3. In addition, Pt $4d_{5/2}$ and Sn 3d profiles are displayed in Figs. 12 and 13, respectively. The Pt $4d_{5/2}$ emission showed a single peak at
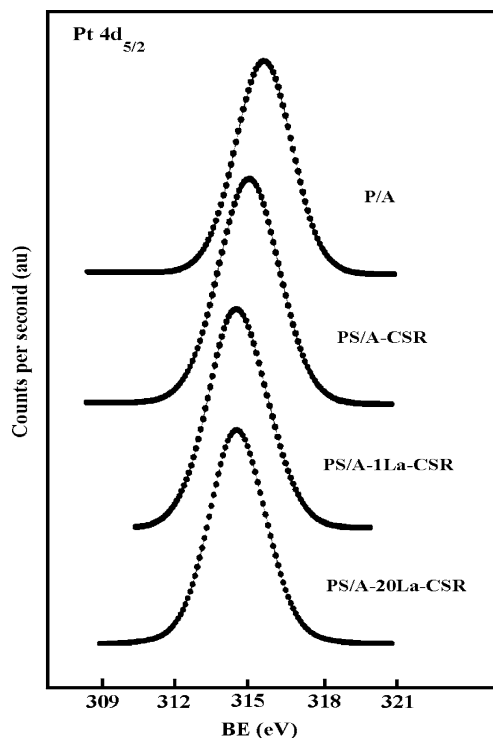
Fig. 12. Pt $4d_{5/2}$ Core level spectra of P/A, PS/A–CSR, PS/A–1La–CSR, and PS/A–20La–CSR.

Fig. 13. Sn 3d Core level spectra of PS/A–1La–CSR and PS/A–20La–CSR.

binding energies of 314.6–314.8 eV (Fig. 12), which are characteristic of the zero valence state of Pt [29,30]. In contrast with the samples prepared by the SI methodology, the CSR counterparts exhibit platinum in metallic state even at the highest lanthanum content of 20%. From the Sn 3d profiles (Fig. 13) it is also evident that the most Sn $3d_{5/2}$ peak of tin spectra for PtSn bimetallics supported on lanthanum-modified alumina prepared by CSR procedure showed two components (Table 3, Fig. 13). One component at binding energies of 485.4, 485.5, and 485.2 eV for lanthanum loadings of 1, 10, and 20 wt%, respectively, can be assigned as above to reduced tin either in the metallic (Sn^0) or in the alloyed ($SnPt_x$) state. The other Sn $3d_{5/2}$ component placed at higher binding energies (487.2–488.3 eV) can be ascribed to an oxidized tin species, such as Sn^{2+}. On examining the peak percentages given in parentheses in Table 3, it is clear that the proportion of this oxidized Sn^{2+} species increases from 45 to 65% with increasing lanthanum loading from 1 to 20%. This tendency is also different from that of the catalysts prepared following the SI methodology, which showed an almost constant proportion of Sn^{2+} species (62–68%) irrespective of lanthanum loadings.

Surface atomic ratios were also derived for both catalyst series. For this calculation, peak intensities normalized by atomic sensitivity factors were employed [28]. The Pt/Al, Sn/Al, and La/Al surface ratios for the two SI and CSR catalysts series are compiled in Table 4. For comparison, the tin-free P/A sample was also included in the same table. From these data it is clear that the Pt/Al atomic ratio
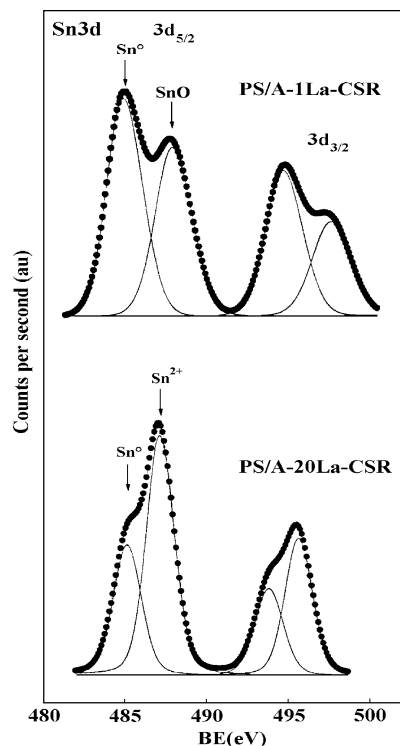
increases with increasing lanthanum content. The strong increase of La/Al atomic ratios for SI and CSR containing 10 and 20% lanthanum suggests that lanthanum could be segregated to the surface. On the other hand, if a comparison is made between Sn/Al ratios for SI and CSR samples, large differences are apparent. One possible explanation for this behavior is that tin is poorly dispersed on the support in the CSR catalyst series.

3.8. Conversion of n-heptane

The activity (rate) and selectivity for n-heptane conversion over Pt and PtSn catalysts are reported in Table 5. A diminution of the activity of the P/A catalyst (21.0×10^{-6} mol/(s g)) with the addition of Sn is observed with both techniques of preparation, successive impregnation (9.9×10^{-6} mol/(s g)) and controlled surface reaction (6.8×10^{-6} mol/(s g)). The decrease in activity with the addition of tin to the P/A catalyst indicates that Sn modifies

Table 4
Surface atomic ratios of supported Pt and Pt–Sn catalysts

Catalyst	Pt/Al at	Sn/Al at	La/Al at
P/A	0.0011	–	–
PS/A–1La–SI	0.0015	0.0173	Traces
PS/A–10La–SI	0.0017	0.0264	0.037
PS/A–20La–SI	0.0063	0.0188	0.118
PS/A–1La–CSR	0.0011	0.0015	0.003
PS/A–10La–CSR	0.0028	0.0006	0.034
PS/A–20La–CSR	0.0051	0.0054	0.112

Table 5
Activity and selectivity of n-heptane conversion over Pt and PtSn supported on γ-Al$_2$O$_3$ and γ-Al$_2$O$_3$–La catalysts

Catalyst	Pt	Sn	Rate	Selectivity (%)				
	(wt%)		($\times 10^6$ mol/(s g))	C$_1$–C$_6$	Benzene	iC$_7$	C$_7$$^=$	Toluene
P/A	0.49	–	21.0	25.7	1.8	18.3	31.0	23.2
PS/A–SI	0.37	0.51	9.9	21.7	3.6	10.9	21.8	42.0
PS/A–1La–SI	0.45	0.27	6.6	20.7	2.1	10.2	35.0	32.0
PS/A–10La–SI	0.38	0.43	3.0	15.4	2.0	4.8	47.8	30.0
PS/A–20La–SI	0.44	0.38	0.04	14.6	0.0	0.0	59.8	25.6
PS/A–CSR	0.46	0.11	6.8	8.6	1.34	14.4	29.0	46.7
PS/A–1La–CSR	0.5	0.08	3.2	9.5	1.1	8.7	36.7	44.0
PS/A–10La–CSR	0.38	0.10	1.5	10.7	1.0	10.9	39.8	37.6
PS/A–20La–CSR	0.46	0.13	2.3	11.4	1.1	6.7	48.8	32.0

C$_1$–C$_6$: hydrocarbons. iC$_7$: C$_7$ isomers. C$_7$$^=$: C$_7$ olefins.

the platinum activity. For SI preparations, additionally, such activity is lower in PtSn/Al$_2$O$_3$–La catalysts. It becomes minimal at the highest La loads, 0.04×10^{-6} mol/(s g) for the PS/A–20La–SI catalyst.

Selectivity was also modified in Pt–Sn/Al$_2$O$_3$–La–SI catalysts. Hydrogenolysis, n-alkane isomerization, benzene, and dehydrocyclization products were diminished. However, a noticeable increase of C$_7$-olefin formation was observed in PS/A–20La–SI catalyst.

For CSR preparations, the effect of lanthanum content on activity is less noticeable. The activity values are 3.2, 1.5, and 2.3×10^{-6} mol/(s g) for 1, 10, and 20 wt% La, respectively. In these catalysts the selectivity to hydrogenolysis, n-alkane isomerization, and aromatization is less affected by lanthanum. Nevertheless, as was reported for SI preparations, a high selectivity to C$_7$-olefins was obtained.

4. Discussion

Electron micrographs shown that platinum particle size is not modified by the addition of tin or by the presence of lanthanum in the support. The mean particle size observed by conventional and HREM microscopy is around 2.4 nm on the three selected catalysts. Therefore we can discard platinum particle size effects on activity, and hence the selectivity behavior observed on Pt–Sn/Al$_2$O$_3$–La catalysts can be attributed to tin and/or lanthanum effects over platinum. The constant platinum particle size in the catalysts studied can be due to the low platinum content (0.5 wt%) supported over alumina with high specific surface area (221 m^2/g).

The essential difference between the two preparation methods is the way in which tin was added to Pt/γ-Al$_2$O$_3$ and Pt/γ-Al$_2$O$_3$–La$_2$O$_3$ catalysts. For SI preparations tin was added by impregnating the Pt-supported catalyst with a SnCl$_4 \cdot$ 5H$_2$O solution, giving catalysts in which tin covers mainly the support (0.5 Sn wt%).

For the CSR preparations, tin was deposited under controlled conditions; i.e., a selective surface reaction between the hydrogen adsorbed on platinum and the organotin compound, Sn(n-C$_4$H$_9$)$_4$, was carried out. Then in these catalysts tin must be found mainly over the platinum particles.

The addition of Sn by SI leads to random deposition of Sn preferentially over the support. A comparison of the activities of cyclohexane dehydrogenation of Pt/Al$_2$O$_3$ catalyst with those of Pt–Sn/Al$_2$O$_3$–SI reveals that the activities are on the same order. Here, we can assume that Sn could be found on the interface of platinum and support and therefore a close contact between platinum, tin, and lanthanum oxides could be achieved. As has been observed in CO-FTIR and XPS spectra, in SI catalysts the Pt in the oxidized state increases with the amount of lanthanum due to the Pt–SnO$_x$–La$_2$O$_3$ interaction where Pt^{2+} is stabilized. Then the decrease in activity for cyclohexane dehydrogenation in lanthanum content catalysts can be explained by a loss of dehydrogenation activity of Pt due to the formation of Pt^{2+} on the bimetallic particles (Table 1).

In PtSn–CSR catalysts Sn was deposited preferentially over the surface of platinum [18]. The Sn content is almost the same in all catalysts (0.08–0.13 wt%), with and without lanthanum, and the accessible surface of Pt is reduced in the same proportion in all catalysts. This explains the constant values for the activity of cyclohexane dehydrogenation obtained with these preparations. In these catalysts, in opposite to SI preparations, the close contact between Pt, Sn, and La$_2$O$_3$ is largely minimized.

Such results led us to propose two models for Pt–Sn/ γ-Al$_2$O$_3$–La bimetallic catalysts prepared by successive impregnation and control surface reaction; see Figs. 14, 15. In Fig. 14 (SI preparations), it is proposed as being responsible for the activity and selectivity behaviors in the formation of the multiple interface SnO–La$_2$O$_3$–Al$_2$O$_3$ which stabilizes Pt^{2+}. For CSR preparations as shown in Fig. 15, the main effect of tin is related to the dilution of the platinum particles forming Pt–Sn alloys.

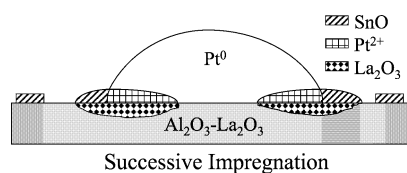Fig. 14. Schematic model of PtSn bimetallic particles supported on γ-Al$_2$O$_3$–La$_2$O$_3$ and obtained by the successive impregnation method.
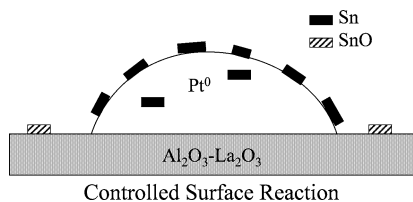
Fig. 15. Schematic model of PtSn bimetallic particles supported on γ-Al$_2$O$_3$–La$_2$O$_3$ and obtained by the controlled surface reaction method.

For n-heptane conversion, the diminution of activity of both Pt–Sn/Al$_2$O$_3$–La catalysts series, if compared with that of the Pt/Al$_2$O$_3$ catalyst, could be discussed with the same arguments used for cyclohexane hydrogenation.

Selectivity in the n-heptane conversion was also modified by the method of tin addition to the Pt/Al$_2$O$_3$–La catalysts. The effect of Sn on the catalytic properties of Pt/Al$_2$O$_3$ can be observed mainly in reactions that depend on the metallic phase. The main effect observed with the Sn addition to platinum is the diminution of the carbon–carbon bond hydrogenolysis reaction in both preparations. However, this decrease toward C$_1$–C$_6$ selectivity is more important for catalysts prepared by CSR: it goes from 25.7% for P/A to 8.6% for PS/A–CSR catalyst. Here we are in the presence of dilution effect of Pt ensembles. This reduction of large Pt atoms ensembles caused by Sn^0 explains the diminution of deep hydrogenolysis in n-heptane conversion according to an ensemble effect [32,33]. The decrease in hydrogenolysis is observed to a lower extent on the PS/A–SI catalyst, since in this preparation tin would be deposited mainly on the support.

However, both preparations showed a high production of C$_7$-olefins, 59.8 and 48.8% at loads of 20% La for SI and CSR catalysts, respectively. It seems that two effects operate here. The FTIR spectra of pyridine adsorbed on the supports showed an important decrease in the support acidity with La loads (Fig. 7). This modification of the surface acidity on the support could have an effect on the bifunctional reactions (loss of support acidity). On the other hand, in both preparations we observed a loss in hydrogenation–dehydrogenation activity (metal function) [13]. The olefin formed on the metal in both preparations could not be isomerized on the support and then it desorbed before being hydrogenated, giving large selectivity to C$_7$-olefins. The large selectivity to olefins found in Pt–Sn/Al$_2$O$_3$–La catalysts is an important result because, as is well known, olefins are important raw materials in the petrochemical process.

5. Conclusions

The effect of tin on the catalytic properties of PtSn/γ-Al$_2$O$_3$–La substrata depends on the method of tin deposit: either successive impregnation or controlled surface reaction. For catalysts prepared by SI, FTIR spectroscopy of CO adsorption and XPS spectroscopy revealed that the Pt–SnO–La$_2$O$_3$ multiple phases interact and Pt is stabilized as Pt^{2+}.

In contrast, for catalysts prepared by CSR, selective deposition of Sn on the surface of platinum particles does not favor such interaction and Pt remains as Pt^0. Also observed was an acidity drop of the γ-Al$_2$O$_3$ support with lanthanum content.

The loss in metallic character of platinum in La–SI catalysts causes an activity decrease in the dehydrogenation of cyclohexane and n-heptane conversion as function of lanthanum load. Total inhibition of benzene formation at high La content, as well as diminution of hydrogenolysis products and an important increase in the olefins, was observed.

For CSR preparations no variation in activity of cyclohexane dehydrogenation and n-heptane conversion as function of lanthanum was observed. High selectivity toward olefins and low hydrogenolysis products was obtained.

References

[1] F.M. Dautzemberg, H.W. Kouenkoven, German Offenlegungss Chrift 153 (2) (1972) 891.
[2] J.K.A. Clarke, Chem. Dev. 75 (1975) 391.
[3] E.O. Box, L.E. Drehman, F. Farha, German Patent 2,127,353, 1970.
[4] M.E. Olbrich, D.L. McKay, D.P. Montgomery, US Patent 4,926,005, 1989.
[5] F.C. Wihelm, US Patent 3,755,480, 1973.
[6] F. Humblot, J.P. Candy, F. Le Peltier, B. Didillon, J.M. Basset, J. Catal. 179 (1998) 459.
[7] J. Salmones, J. Wang, J.A. Galicia, G. Aguilar Rios, J. Mol. Catal. A 184 (2002) 203.
[8] A. Vázquez-Zavala, A. Ostoa-Montes, D. Acosta, A. Gómez-Cortés, Appl. Surf. Sci. 136 (1998) 62.
[9] O.A. Barias, A. Colmen, E. Belkan, J. Catal. 158 (1996) 1.
[10] G. Meitzner, G.H. Via, F.W. Lytle, S.C. Fung, J.H. Sinfelt, J. Phys. Chem. 92 (1998) 2925.
[11] Y.X. Li, K.J. Klabunbe, B.H. Davis, J. Catal. 128 (1991) 1.
[12] F. Oudet, P. Courtine, A. Vejux, J. Catal. 114 (1988) 112.
[13] G. Del Angel, G. Torres, V. Bertin, Stud. Surf. Sci. Catal. 130 (2000) 2531.
[14] A. Vázquez, T. López, R. Gómez, X. Bokhimi, J. Mol. Catal. A 167 (2001) 91.
[15] G. Del Angel, A. Bonilla, J. Navarrete, E.G.J. Figueroa, J.L.G. Fierro, J. Catal. 203 (2001) 257.
[16] Ch. Travers, J.P. Bournoneville, G. Martino, in: Proc. 8th International Congress on Catalysis, Vol. IV, Berlin, 1984, p. 891.
[17] J. Margitfalvi, S. Szabo, F. Nagy, in: I. Cerveny (Ed.), Catalytic Hydrogenation, Elsevier, Amsterdam, 1986, p. 373.
[18] H.R. Anduriz, P. Bodnariuk, B. Coq, F. Figueras, J. Catal. 119 (1986) 97.
[19] K. Kili, F. Le Normand, J. Mol. Catal. A: Chemical 140 (1999) 267.
[20] D.I. Kondaries, X.E. Verykios, J. Catal. 174 (1998) 52.
[21] E. Rogemond, N. Essayem, R. Frety, V. Perrichon, M. Primet, F. Mathis, J. Catal. 166 (1997) 229.
[22] F. Fajardie, J.F. Tempére, G. Djèga-Mariadassou, G. Blanchard, J. Catal. 163 (1996) 77.

[23] J. Ward, in: J.A. Rabo (Ed.), Zeolite Chemistry and Catalysis, in: ACS Monograph, Vol. 171, Am. Chem. Society, Washington, DC, 1976.

[24] L.Ch. De Ménorval, A. Chaqroune, B. Coq, F. Figueras, J. Chem. Soc. Faraday Trans. 93 (20) (1997) 3715.

[25] R.J. Irving, E.A. Magnusson, J. Amer. Soc. (1958) 2283.

[26] M. Primet, J.M. Basset, M.V. Mathieu, M. Prettre, J. Catal. 29 (1973) 231.

[27] R. Queau, D. Labroue, R. Poilblanc, J. Catal. 69 (1981) 249.

[28] D. Briggs, M.P. Seah (Eds.), Practical Surface Analysis by Auger and X-Ray Photoelectron Spectroscopy, Wiley, Chichester, 1983.

[29] L. Guczi, G. Lu, Z. Zsoldos, Catal. Today 17 (1993) 459.

[30] K. Okada, A. Kotani, J. Phys. Chem. Jpn. 61 (1992) 449.

[31] C. Larese, J.M. Campos-Martin, J.J. Calvino, G. Blanco, J.L.G. Fierro, C.Z. Kang, J. Catal. 208 (2002) 467.

[32] J.M. Parera, J.N. Beltramini, J. Catal. 112 (1988) 357.

[33] B. Coq, B. Chaqroune, F. Figueras, B. Nciri, Appl. Catal. 82 (1992) 231.